Development of high-density helicon plasma sources and their applications[a)]

Shunjiro Shinohara,[1,b)] Tohru Hada,[1] Taisei Motomura,[1] Kenji Tanaka,[1] Takao Tanikawa,[2] Kyoichiro Toki,[3] Yoshikazu Tanaka,[3] and Konstantin P. Shamrai[4]
[1]*Interdisciplinary Graduate School of Engineering Sciences, Kyushu University, 6-1 Kasuga Koen, Kasuga, Fukuoka 816-8580, Japan*
[2]*Research Institute of Science and Technology, Tokai University, 1117 Kitakaname, Hiratsuka, Kanagawa 259-1292, Japan*
[3]*Institute of Symbiotic Science and Technology, Tokyo University of Agriculture and Technology, 2-24-16 Naka-cho, Koganei, Tokyo 185-8588, Japan*
[4]*Institute for Nuclear Research, National Academy of Sciences of Ukraine, 47 Prospect Nauki, Kiev 03680, Ukraine*

(Received 5 December 2008; accepted 17 February 2009; published online 28 April 2009)

We report on the development of unique, high-density helicon plasma sources and describe their applications. Characterization of one of the largest helicon plasma sources yet constructed is made. Scalings of the particle production efficiency are derived from various plasma production devices in open literature and our own data from long and short cylinder devices, i.e., high and low values of the aspect ratio A (the ratio of the axial length to the diameter), considering the power balance in the framework of a simple diffusion model. A high plasma production efficiency is demonstrated, and we clarify the structures of the excited waves in the low A region down to 0.075 (the large device diameter of 73.8 cm with the axial length as short as 5.5 cm). We describe the application to plasma propulsion using a new concept that employs no electrodes. A very small diameter (2.5 cm) helicon plasma with 10^{13} cm^{-3} density is produced, and the preliminary results of electromagnetic plasma acceleration are briefly described. © *2009 American Institute of Physics*.
[DOI: 10.1063/1.3096787]

I. INTRODUCTION

In the modern world, plasma science has gained great importance in many aspects, and research in this area has created an abundance of new fields. One of the great achievements in the field is the clarification of a variety of plasmas, leading to the realization that the basic ideas of plasma physics share much in common and are interconnected to each other in many areas. Plasma science played an important role in nonlinear physics, and, at the same time, its understanding has led to new applications and industrial products.

In any field of research, developing a plasma source suited to the field is crucial and indispensable, and advances in many areas have been made. For example, in fields such as the application of plasmas, fusion, and basic fields including space plasmas, it is important to construct high-density plasma sources. Low temperature and low pressure helicon plasma sources[1–5] are one of the promising sources due to their easy operation over a wide range of operational parameters under a current free condition, where the helicon wave is a bounded wave in the whistler wave range of frequencies (between the ion and electron cyclotron frequencies) with both right- and left-handed circular polarizations.

We have developed uniquely featured helicon plasma sources and have currently characterized up to seven devices with, for example, very large[6–10] or very small scales,[11–17] or very strong magnetic fields.[18] We have also developed sources that are used for fundamental and applied investigations. Before the use of the spiral antenna,[19–21] few attempts were made using various shapes of antennas such as loop, helical, saddle coil types[2,5] to produce a large scale plasma, i.e., diameter typically larger than 10 cm. Using a spiral antenna, plasma with a density in the range of 10^{11}–10^{12} cm^{-3} was produced under a weak magnetic field[19] in a short chamber (25 cm long, 48 cm in diameter).

High-density ($\sim 10^{13}$ cm^{-3}) plasma experiments performed at Kyushu University[20,21] used a vacuum vessel, 45 cm in diameter and 170 cm in axial length, by using a spiral antenna. With this large device, in addition to the basic studies on helicon/whistler wave characteristics in the high-density regime,[22–26] many fundamental and applied studies have been done in the low-density region by voltage biasing of the concentric electrodes located at the end of the vessel. These include the control of the radial density profile and the high azimuthal plasma rotation with a high velocity shear,[27–32] a proof of principle experiment on ion mass separation,[33] and the self-excited, density-transition phenomenon in the bistable system.[28,34,35] Using this device with the plasma diameter reduced to 5 cm (the axial length was maintained at 170 cm), we have characterized in detail the high-density helicon production and radio frequency (rf) wave phenomena,[36–43] which included the analyses of various antenna geometries. Drift wave turbulence, which is important for transport phenomena in magnetic confinement devices and for an understanding of fundamental processes, has been

[a)]Paper TI1 2, Bull. Am. Phys. Soc. **53**, 238 (2008).
[b)]Invited speaker. Electronic mail: sinohara@aees.kyushu-u.ac.jp.

extensively investigated using a plasma diameter of 10 cm with the above device and the modified device.[44–56] Using the helicon wave production scheme this turbulence study is being actively pursued in many other linear devices, e.g., Refs. 57–59, as well as the stellarator device, e.g., Ref. 60. There are now a variety of extensive studies on helicons covering fields both fundamental and applied: for example, the development and the characterization of helicon plasma sources including the wave structures, the generation mechanisms, and the instabilities (e.g., recent references of Refs. 61–64 in addition to those given above in this paragraph). Other studies deal with emission rate coefficients,[65] neutron sources,[66] nuclear waste treatment,[67] plasma propulsion[68–70] (which will be discussed later), double layer formation relating to this propulsion,[71] high beta plasma with instabilities,[72,73] and Alfvén wave excitation.[74] In addition there are studies on various industrial plasma processing technologies such as etching.[75]

After developing the large diameter device[20,21] that employs the spiral antenna, we constructed three additional devices. The first has an inner vessel diameter of 20 cm (Refs. 76–78) and uses an advanced segmented multiloop antenna. The second has an inner diameter of 40 cm (Refs. 79 and 80) and uses the above-mentioned spiral antenna. The third has an inner diameter of 73.8 cm (Refs. 6–10) and uses a flexible combination of four-turn spiral antenna. As was mentioned, a large volume, high-density helicon plasma source is very useful for many fundamental and applied studies, and our device[6–10] named Large Helicon Plasma Device (LHPD) with its 73.8 cm diameter and 486 cm the axial length is the largest volume (2.1 m^3) helicon plasma device yet developed as far as we know. Note that the device volume of the Archimedes Technology group device[67] is larger than ours, but the substantial plasma volume (<2 m^3) is slightly less than ours because its plasma diameter D is <80 cm and its axial length L is 389 cm. On the other hand, since a short axial length combined with a large diameter is important for applications such as industrial plasma processing and magnetoplasma rockets, high-density plasma production in a device with a low aspect ratio A (A: ratio of the axial length to the diameter) should be investigated, and detailed characterization of the plasma profile and wave structures should be done. It is also important for future device design to study particle production scaling as a function of geometrical size, i.e., diameter and axial length.

Developing a small helicon plasma source is also important, since this type of device has many applications, including plasma processing and plasma propulsion. We developed, to our knowledge, the smallest diameter ($D=2.5$ cm),[11–17] smallest volume (23 cm^3) helicon plasma source (axial length $L=4.7$ cm).[11] We note that others have reported on small-volume helicon plasma production ($D=4.5$ cm and L is from 10 to 65 cm),[81,82] and results indicated the standing wave rf field patterns in the case of short axial length. In this report, we focus on efficient plasma propulsion by the new method of using the electromagnetic force in the developed high-density helicon plasma source with a concept of no electrodes. Electric propulsion by plasmas is regarded as a promising scheme in space applications due to its superior capacity to conserve propellant compared to the chemical propulsion techniques. This has led, for example, to the Variable Specific Impulse Magnetoplasma Rocket (VASIMR^{TM}) project[68] that uses ion cyclotron heating for the helicon plasma acceleration in the presence of the divergent magnetic field (electrothermal acceleration by magnetic nozzle expansion), as well as the Mini-Magnetospheric Plasma Propulsion (M2P2)[69] that uses solar wind and inflation of a helicon plasma in a dipole magnetic field. Since electric propulsions are employed for long-term missions, the operating lifetime of a plasma acceleration device must be long and the efficiency high. Our proposed electrodeless high-density helicon plasma production device is hence very attractive, because its weak plasma-wall interactions lengthen its operating lifetime, making it an efficient plasma production and propulsion scheme.

In this paper, we give experimental results from the two high-density helicon plasma sources mentioned above. The first is a very large diameter source with a very small aspect ratio (as small as 0.075). This device of LHPD is also interesting from the viewpoint of the imposed axial boundary conditions and particle production scaling. The second device is a very small diameter source with which we conduct a plasma acceleration trial in the high-density condition ($\sim 10^{13}$ cm^{-3}).

This paper is organized as follows. In Sec. II, the experimental setup of the large diameter device LHPD is described. We then characterize the low aspect ratio plasma production and discuss particle production scaling along with the underlying physics. In Sec. III, we describe the setup of the small helicon plasma source, and the first trial of electromagnetic plasma acceleration. We then discuss high-density helicon plasma production, following which we give a brief analysis. Finally, conclusions are given in Sec. IV.

II. LARGE DIAMETER EXPERIMENT

A. Experimental setup

Our experiments at the Institute of Space and Astronautical Science, Japan Aerospace eXploration Agency (ISAS, JAXA) were performed in a vacuum chamber, 75 and 73.8 cm in outer diameter and inner diameter, respectively, and 486 cm in axial length [see a schematic of LHPD in Fig. 1(a)].[6–10] In order to shorten the axial plasma length, we installed an electrically floating termination plate: made of a stainless steel (SUS) punching plate, 54 cm in diameter with 0.05 cm thickness, and with a geometrical transparency of 35% (each hole diameter is 0.15 cm). The reason why we use the punching plate is to accommodate future propulsion schemes such as electrostatic acceleration utilizing this as an electrode. The punching plate also has the advantage of conducting a measurement of that is rf-free and quiet in the outer source region separated from the source region by the plate, although the plasma density in the outer source region is lower compared with the source region itself. A uniform magnetic field in the central region that is over 2 m in the axial direction [see Fig. 1(b)] is produced by 14 main coils. The main coil current of $I_m=50$ A corresponds to a magnetic field strength of 140 G. Due to the lack of coils at both ends

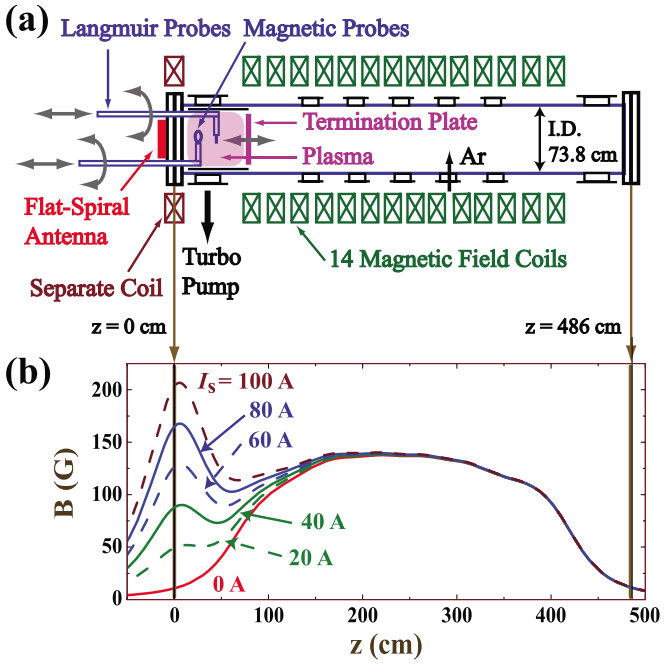

FIG. 1. (Color online) (a) Schematic of the large volume, large diameter helicon plasma device LHPD at ISAS, JAXA. (b) Axial magnetic field configurations for various values of the separate coil current I_s at radial position $r=0$ cm.

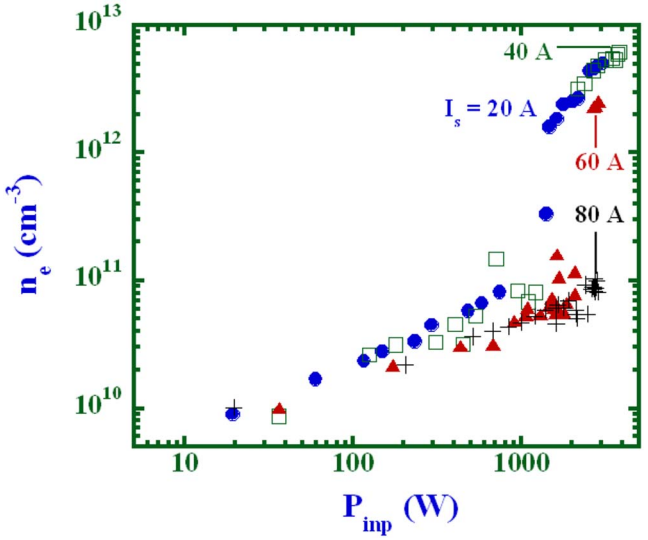

FIG. 2. (Color online) Electron density n_e as a function of the rf input power P_{inp} with the axial length of $L=81$ cm for various values of the separate coil current I_s: 20, 40, 60, and 80 A with an argon gas pressure P_{Ar} of 0.75 mTorr. A Langmuir probe is located at the axial position of $z_p=45$ cm.

of the device, the magnetic field is weaker and nonuniform in these regions. To compensate for the weak magnetic field near the spiral antenna located at one end of the chamber, a separate coil with an independent power supply is additionally installed there [see the left-hand side of the chamber in Fig. 1(a)]. Note that the separate coil current, I_s, does not significantly alter the main central magnetic field generated by I_m. The base pressure of our device is $\sim 10^{-7}$ Torr, achieved using a turbomolecular pump at a pumping speed of 1800 l/s. Typically, argon (Ar) is used as the working gas. It is fed through a needle valve with a fill pressure, P_{Ar}, of 0.75–7.5 mTorr. In this experiment, 0.75 mTorr is used unless otherwise specified.

Next, we briefly describe the rf system[6] used in our experiment. The spiral antenna, which is expected to excite the azimuthal mode number $m=0$, is located outside the quartz window of the vacuum chamber, and has four turns with 43 cm outer diameter. It has taps for electrical connections at every half turn. Any two connection points can be chosen to feed in the rf power so that the antenna radiation field pattern may be varied easily. Altering the radiation pattern, in turn, causes a change in the plasma production process,[6–10] making it possible to control the radial plasma density profile, which can also be controlled by changing the magnetic field configuration near the excitation antenna by varying the separate coil current I_s. The maximum output power of the rf amplifier is 5 kW and its frequency f is typically 7 MHz. The rf system is operated in pulsed mode in which a typical pulse width is 12–40 ms and the repetition rate is 1 Hz.

The spatial plasma parameters, such as plasma density n_e and electron temperature T_e (typically 3–5 eV), are measured by scanning two Langmuir probes (one-sided tungsten disk probes of 0.2–0.5 cm in diameter) inside the chamber. The excited rf wave field patterns are measured by two single-turn magnetic probes approximately 1 cm in diameter, constructed from semirigid coaxial cables. These Langmuir and magnetic probes are inserted through the end flange on the antenna side [see Fig. 1(a)], and the probe shafts are bent 90° with respect to the chamber axis so that they can be rotated to measure radial profiles, and can be translated axially to measure axial profiles. Ordinary digital cameras are used to monitor the plasma light. Observation windows are located on the end flanges at both ends of the chamber and also on the side of the chamber at $z=31.5$ cm.

B. Plasma production and scaling

We study the electron density n_e as a function of the rf input power P_{inp}, by reducing the axial length L from 486 cm (full length) to 81 cm, and changing the separate coil current I_s, as shown in Fig. 2. After the so-called, density jump, n_e is greater than 2×10^{12} cm^{-3} with $P_{inp}\sim 3$ kW (note that the threshold rf power for this jump increases with I_s). For the case of $I_s=80$ A, no density jump is found even with P_{inp} close to 3 kW. This magnetic field dependence near the antenna is consistent with the previous results obtained with a long axial length of 486 cm,[6–9] and can be understood as arising from the power balance between the plasma loss and the rf input power and described using a simple model of the dependence of the antenna loading on the plasma density, changing the magnetic field.[26,41,42] The plasma density n_e is close to 10^{13} cm^{-3} for $L=486$ cm with $P_{inp}\sim 3$ kW, but decreases gradually with reducing L at the same input rf power.[10]

Figure 3 shows the dependence of n_e on P_{inp} for a very short axial length L of 5.5 cm. Here, the aspect ratio A is 0.075, using the device diameter of 73.8 cm. Although such a small axial length is expected to cause a large axial loss, we still observe a relatively high density with n_e

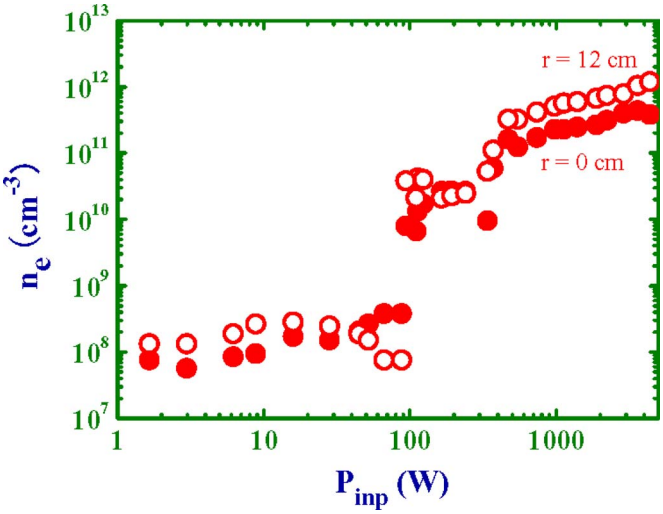

FIG. 3. (Color online) Dependence of n_e on P_{inp} with L=5.5 cm, I_s =20 A, and P_{Ar}=1.5 mTorr. A Langmuir probe is at z_p=3.8 cm.

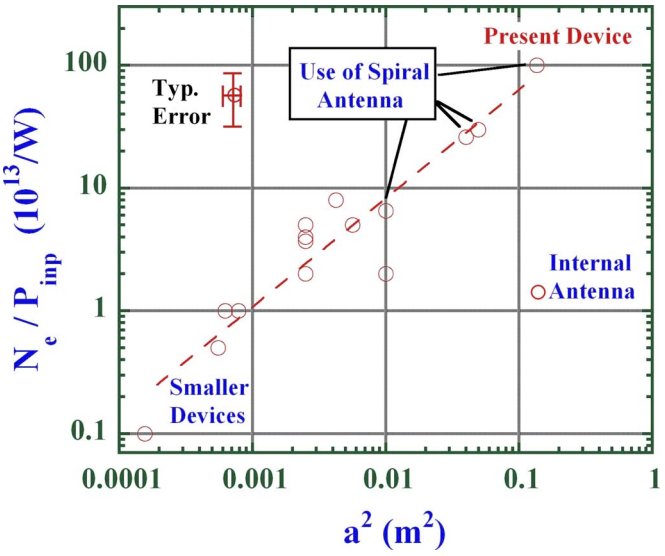

FIG. 4. (Color online) Relationship between N_e/P_{inp} and a^2 using various device data. Here, N_e, P_{inp}, and a show the total number of electrons produced, input rf power, and the plasma radius, respectively. A least square fitting curve in the power series (broken line), $N_e/P_{inp} \propto a^{2\times 0.88}$ with a correlation coefficient of 0.99, is also shown.

$\sim 10^{12}$ cm^{-3} (particle production efficiency will be discussed later). Note that in this case, a mostly hollow radial density profile is found, as the density in the center is lower than that at the radius r=12 cm, as can be seen from this figure.

For the case of L=12.5 cm, the radial density profile, be it hollow or relatively flat near the plasma center, is dependent on P_{inp}. There is a tendency, along the z axis, for the radial density profile to be hollow near the antenna and to peak away from the antenna. This can be understood partly from the numerical simulation,[26] which indicates that the absorption power is maximum near the half radius of the antenna but not along the z axis ($r\sim 0$), and that the radial diffusion smears out the hollow profile as z increases. As is the case of L=486 cm, n_e on the order of 10^9 cm^{-3} is produced with only $P_{inp}\sim 1$ W for L=12.5 cm. This corresponds to a very low input power density of 3 μW/cm^3, and yet, regardless of the axial length, the plasma is still produced with a density on the order of 10^8–10^9 cm^{-3}.

We now consider the particle production efficiency N_e/P_{inp}, where N_e is the total number of electrons in the entire plasma region. The estimation of this efficiency is useful for understanding or checking plasma production condition in each device and for future device designs. First, we treat the long cylinder case, where the aspect ratio A is large, with a relatively weak magnetic field so that ions are weakly magnetized. This leads to the condition that the ion radial loss dominates (electrons flow along the axis but the flow speed is lowered by the total ambipolarity condition arising from the slower radial loss rate of ions). In this case, from Ref. 9, N_e/P_{inp} is expected to be proportional to a^2, and in another expression n_e is inversely proportional to L. Figure 4 shows the relationship between N_e/P_{inp} and a^2, using data from various devices, which is in good agreement with this linear scaling over a wide diameter range. Here, we have added the data[13,45,52,67,76–80] (five data points) to those in Fig. 8 of Ref. 9.

Note that the right bottom data point[67] in Fig. 4 deviates from this linear scaling, showing a production efficiency inferior by two orders of magnitude compared with what we achieve with L=486 cm. This may be due to the use of an internal antenna, where the penetration of the electric field excited from the outer radial region toward the plasma center is rendered difficult due to the large diameter. In addition, plasma-antenna interactions and capacitive antenna coupling are strong. Indeed, a previous internal antenna experiment also showed lower production efficiency in another device.[83] This is in contrast to the spiral antenna case, where the electric field easily penetrates to the central region. In addition, since the spiral antenna is located outside a quartz window at the end of the vessel, control of the radial density profile is made possible by the radiation field pattern of this antenna.[6–10] The production efficiencies of our four device experiments using spiral antennas are plotted in the right top region of Fig. 4, and show the excellent production efficiencies of up to 10^{15} particles/W. This scaling shows roughly the upper limit of the plasma production efficiency as long as the above long cylinder (high aspect ratio) condition applies, since the coefficient of proportionality for the ideal case (which is based on the classical collisional diffusion) exceeds the experimental values by a factor of $\sim$3, which is derived using the experimental values from the spiral antenna cases.

We now consider the short cylinder case, where, in contrast to the long cylinder case, the ion particle loss dominates along the z axis: A is small with the magnetic field relatively strong. In this case, from Ref. 9, N_e/P_{inp} is expected to be proportional to L, and n_e inversely proportional to a^2 in another expression. Using our large diameter (73.8 cm) device in conjunction with the termination plate, we produce high-density plasmas with densities on the order of 10^{12}–10^{13} cm^{-3} for the various axial lengths with I_s=0 to 60 A. Figure 5 shows the experimental relationship between N_e/P_{inp} and L, with a linear fit to the three short axial length points. Evidently, linear scaling remains valid for the cases of very short axial lengths, and again the linear coefficient

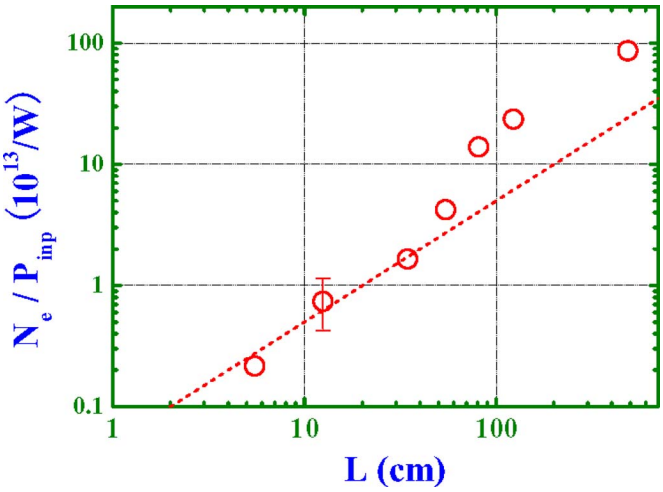

FIG. 5. (Color online) Relationship between N_e/P_{inp} and the axial length L, changing the position of the termination plate. Here, a linear curve is also shown.

for the ideal case is larger than the experimental values by a factor of ~3. In the longer axial length cases, N_e/P_{inp} exceeds this scaling because this is a transition region between the dominant ion loss mechanism being axial and radial. Note that in the short case of $L=12$ cm, this efficiency N_e/P_{inp} in the inductively coupled plasma[1,84] (ICP) (no magnetic field) is nearly the same as the helicon wave plasma case ($I_s=0-60$ A) with the same axial length. ICP results in wave damping (evanescent wave) on the order of the skin depth along the axis, which is stronger than for the helicon wave. Therefore, for the case of the longer axial length case the ICP plasma density is lower than the helicon plasma density at the same rf power, and the ICP density decays rapidly along the axis.[7] In other devices with relatively short axial lengths, this scaling also holds good (device diameter of 48 cm and plasma axial length of 22.4 cm),[19] but the experimentally obtained N_e/P_{inp} (diameter of 4.5 cm and axial length of 10–65 cm) (Refs. 81 and 82) is lower than the expected scaling value by up to approximately one order of magnitude. One of the reasons of this poor efficiency may be the large radial loss due to the small diameter and some instabilities that should be considered in addition to the axial loss.

C. rf wave structures

For the case of short axial length where the axial plasma length is comparable to the axial wavelength of the helicon wave, axial boundaries on both ends of the wave fields must be considered. On the termination plate, which in our experiments is a punching plate made of SUS, the nearly conducting boundary condition for the axial component of the rf magnetic field is expected, i.e., $B_z \sim 0$ (fixed boundary condition). On the inside of the quartz window, a nonconducting, free boundary condition is valid, implying that the axial component of the rf conduction current, j_z, vanishes, or that the rf electric field $E_z \sim 0$. The latter means that B_z is maximum rather than zero on the quartz window. Therefore, the axial mode number of the helicon wave is expected to be

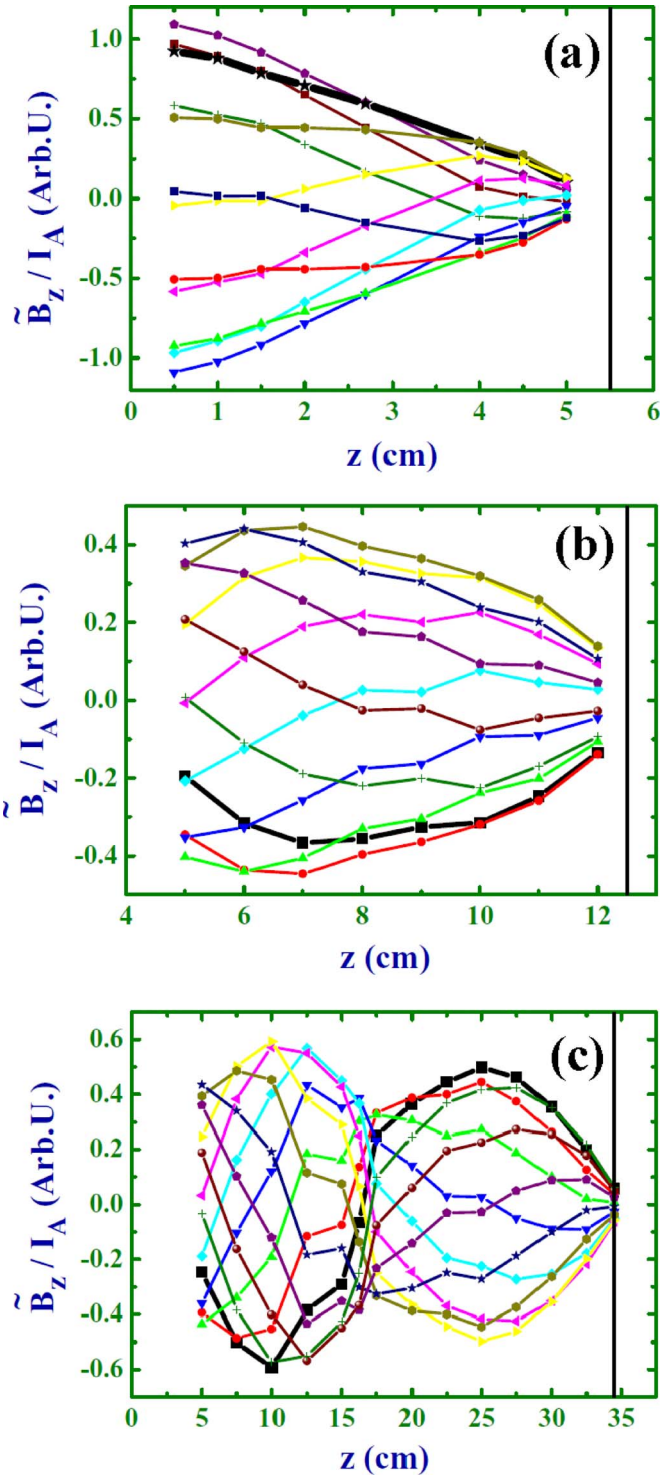

FIG. 6. (Color online) Axial profiles of the ratio of the excited rf magnetic field B_z to the amplitude of the rf antenna current I_A, changing the axial length L: (a) 5.5 cm, (b) 12.5 cm, and (c) 34.5 cm with $P_{\mathrm{inp}} \sim 4$ kW and $I_s=20$ A. Here, the vertical bars show the position of the termination plate.

$n=L/\lambda_z \sim (1/4)+(1/2)p$ $(p=0,1,2,\ldots)$,[86] where λ_z is the axial wavelength. Note that such a mode structure is different from the case when two metal plates are placed on both axial boundaries, which forces the mode number to be $n \sim (1/2)+(1/2)p$.[81,82]

Figure 6 shows the axial profiles of the excited rf magnetic field B_z normalized by the amplitude of the rf antenna

current I_A as a function of the axial length at 12 phases in one rf period. From these data, we see that as L decreases from 34.5 to 12.5 to 5.5 cm, n goes from 5/4 to 3/4 to 1/4, respectively, agreeing with the formula given above. In addition, the observed wavelength is consistent with the helicon wave dispersion relation.[85] Simulations accurately predict these measured axial wave structures for $L=81$ cm (Ref. 10) and $L=54.5$ cm by using the dispersion relation with dampings[85] and assuming a partial wave reflection (~50%) at the termination plate (not shown). In our work, measurement of the wave phase shows that it changes along the z axis near the source region (propagating wavelike), following which the phase change along the axis becomes slower, until finally only a small change is observed near the termination plate (standing wavelike). These observations can be understood as arising from the effect of the reflected wave at the plate. Whether or not the surface waves theoretically predicted near the axial boundary[86,87] exist are left as the subject of a future work.

We now describe the behavior of helicon wave excitation as a function of changing the experimental conditions. For the case of $I_s=20$ A and $L=34.5$ cm, upon decreasing P_{inp} from 4 kW to less than 2 kW, n goes from 5/4 to 3/4 as the plasma density drops, as expected from the helicon wave dispersion relation.[85] For the case of the $L=10$ cm, $n=1/4$ is excited with $I_s=60$ A, but a helicon wave is not excited with $I_s=20$ A, although $n_e \sim 10^{12}$ cm^{-3} is achieved. In this situation, a wave phase change is not observed appreciably along the axis and the apparent wavelength is not consistent with that expected from the dispersion relation. In addition, although a helicon wave with $n=1/4$ (~3/4) is observed in the case of $L=5.5$ (12.5) cm and $I_s=20$ A, these waves are not excited with $I_s=60$ A keeping other parameters constant, and no clear phase change along the axis is found.

Concerning the radial profiles of the excited rf magnetic field B_z, the higher radial modes (second, third, or even higher) are observed in addition to the fundamental radial mode, depending on the magnetic field configuration and the antenna conditions. For instance, the fundamental and second modes dominates for the case of $L=81$ cm and $I_s=60$ A.[10] Although the higher radial modes have also been measured in other experiments,[88–90] the specific mechanism of their excitation is not clear yet, even though the effects of the magnetic field configuration[91] and/or the radial density profile are thought to be important. The inclination of the magnetic field appears crucial for the power absorption profile and the formation of small-scale radial structures. The importance of the radial density profile was ascertained from computations of the radially localized wave eigenmodes in a plasma with a peaked density profile, using the full electromagnetic model that accounts for the Trivelpiece–Gould (TG) waves[86,92] in addition to the helicon waves.[93] In particular, the computations indicate that the peaked radial density profile permits a finite number of pure helicon modes, in contrast with the uniform plasma where only the quasihelicon modes with considerable admixture of the TG waves can exist. It is worth noting that pure helicon modes like those demonstrated above are hard to excite in a standard helicon plasma source because in the latter case there is a wide non-

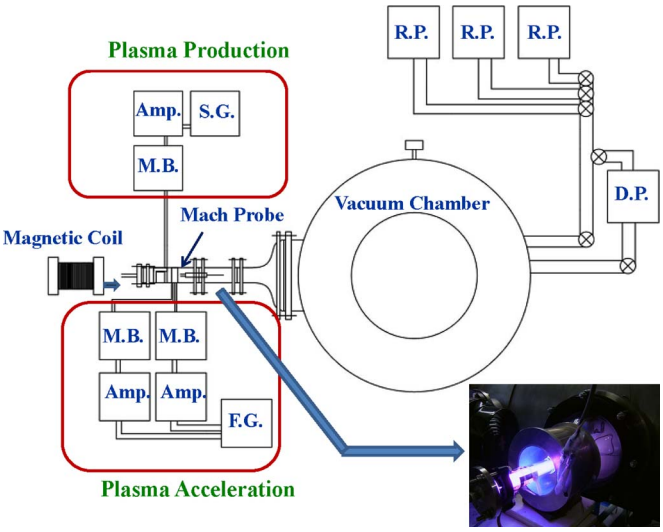

FIG. 7. (Color online) Experimental device at TUAT for the helicon plasma production and the plasma acceleration using very small diameter of 2.5 cm (S.G.: signal generator, F.G.: function generator, Amp.: amplifier, M.B.: matching box, R.P.: rotary pump, and D.P.: diffusion pump).

transparent gap between the antenna and the region where the modes are located. We leave for future research the issues of specific weights (amplitudes) of the different helicon modes in the far field and direct comparison with experimentally measured profiles.

III. SMALL DIAMETER EXPERIMENT

A. Experimental setup

Figure 7 shows the device at Tokyo University of Agriculture and Technology (TUAT) that produces high-density plasmas and electromagnetic acceleration. A Pyrex glass tube 30 cm long with 2.5 cm inner diameter is attached to a large vacuum chamber that has a base pressure of less than 1 mTorr. Argon gas is fed in from the left side of the tube by a mass flow controller. Even with a mass flow rate of 0.5 mg/s, the vacuum chamber pressure remains low of ~1 mTorr, and the pressure inside the Pyrex tube is estimated to be 15 mTorr.

The 10.5 cm coil bobbin allows the application of a magnetic field up to 1.45 kG. The plasma is produced via a saddle coil type antenna (Boswell type[94]), located near the center of the coil bobbin position. The rf power supply for the plasma production is operated at an excitation frequency f of 1–100 MHz and has a maximum power of 500 W. Two types of acceleration antennas are used, whose basic ideas are described later: one with 47-turn loops for the excitation of arbitrary azimuthal current waveforms, and one with four rods to generate a rotating electric field. For electromagnetic acceleration, we use two rf power supplies with f between 1 and 10 MHz with a maximum power of 250 W.

A Mach probe to measure the electron density, the electron temperature, and the plasma flow along the axis is installed 6.5 cm downstream from the edge of the acceleration coil. The probe is similar to the one discussed in Ref. 95. It has two electrodes: one facing upstream and one perpendicular to the axis.

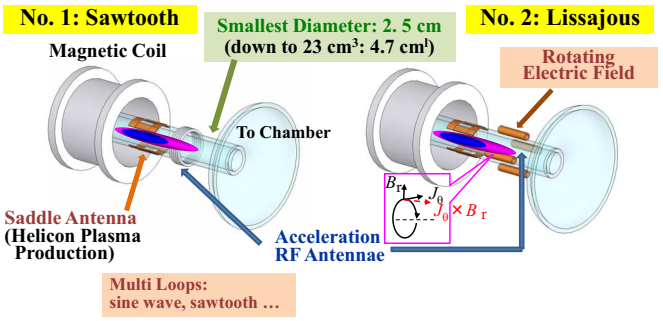

FIG. 8. (Color online) Schematics of the helicon plasma production scheme using the saddle coil, and the plasma propulsion schemes by the multiturn loop antenna for the excitation of the various loop current waveforms (left) and by four rods for the generation of the rotating electric field (right).

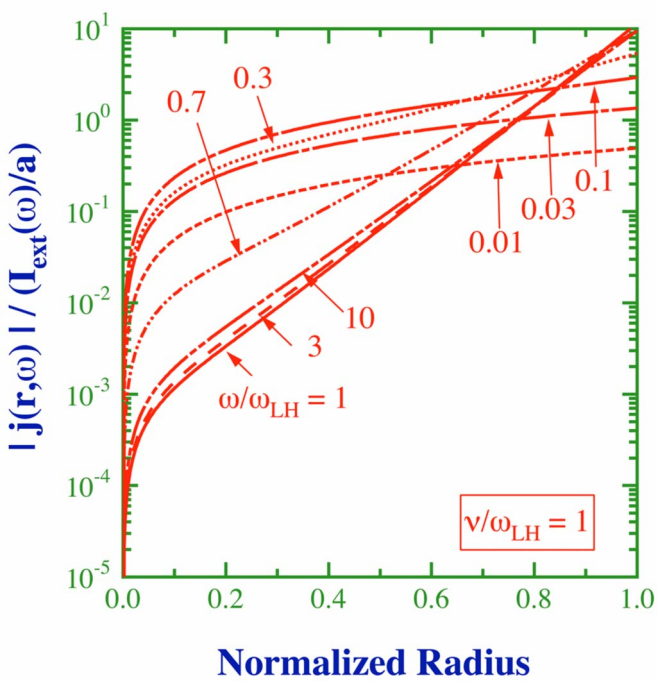

FIG. 9. (Color online) Induced azimuthal current density $|j(r,\omega)|$, normalized by $I_{ext}(\omega)/a$, as a function of the normalized plasma radius r/a, changing the excitation angular frequency ω normalized by the lower hybrid frequency ω_{LH}. Here, ν/ω_{LH} (ν: electron collision frequency) is taken as 1.

B. Brief analysis of the plasma propulsion scheme

We tried two schemes to accelerate the produced plasma along the axis, both of which use the electromagnetic force, $j_\theta \times B_r$ (j_θ is the azimuthal current density, B_r the radial magnetic field). The basic concepts of these methods are shown in Fig. 8. In our cylindrical geometry, the B_r component comes from the static divergent magnetic field generated by external magnets, and the induced j_θ component comes from the external applied electric field (this component is crucial to our study). We first describe the j_θ generation method, which uses multiloops wound around the insulation tube. Following this, we discuss the second method (electric field rotation).

The basic idea of j_θ generation (the first method) is to use, in the presence of a static divergent field, the external azimuthal coil current I_{ext} with $m=0$ and an arbitrary waveform, e.g., sine wave or sawtooth wave, in the rf frequency range. In the plasma region, a simple linear analysis under the straight magnetic field leads to a dispersion relation for an extraordinary wave,[1] that is similar to the helicon wave[85] with an axial wavenumber of zero. For a given sinusoidal I_{ext} with an angular frequency ω excited at the plasma edge ($r=a$), we can derive, using the boundary conditions, the induced current density $j(r,\omega)$ in the plasma through the relation of $j(r,\omega)=C(r,\omega)\ I_{ext}$. Here, $C(r,\omega)$ is the response function and represents the transfer, or coupling, efficiency. Figure 9 shows the estimated radial profile of $|j(r,\omega)|$, normalized by I_{ext}/a, for several different values of ω. Here, ν/ω_{LH} is set to unity and the plasma radius a is ten times v_A/ω_{LH} (for argon ions a is 5.4 cm with $n_e=10^{12}$ cm^{-3} and $B=100$ G), where v_A, ω_{LH}, and ν are the Alfvén velocity, the lower hybrid angular frequency,[1] and the electron collision frequency, respectively. As shown in this figure, for ω/ω_{LH} less (greater) than unity, the excited wave in the plasma is propagating (evanescent), and the wave penetrates in the plasma core with the dissipation due to collisions (penetrates only near the edge). Note that for the weakly (strongly) dissipative case, e.g., $\nu/\omega_{LH}=0.01$ (10), the wave with $\omega/\omega_{LH}<1$ reach (does not reach) the plasma core.

For the case of the divergent magnetic field, assuming that the above discussion under the straight magnetic field is still valid, we can estimate the axial component of the plasma acceleration force. Integrating the $j_\theta(r)\times B_r(r)$ term over the radius in the plasma leads to the net force. In a half rf wave period (in the following half period), a positive (a negative) axial force is expected. If the negative force is suppressed, a net positive force is left. If the negative force is nonzero, the accelerated plasma flow in the negative direction exerts a negative thrust on the spacecraft, leading to a zero net force. In addition, if B_r is proportional to the radius, this positive force calculated increases (is nearly constant) with ω for $\omega/\omega_{LH}<1$ (>1) due to the propagating (evanescent) wave characteristics. Here, an exception is in the region of $\omega\sim\omega_{LH}$. The maximum value of this force normalized by the product of I_{ext} and B_r at the plasma edge is $\sim$0.27. Using the spatially uniform density n_e of 10^{12} cm^{-3} and $\omega_{LH}/2\pi=1$ MHz, this corresponds to a maximum net force of $\sim$25 mN for $I_{ext}=10$ A and B_r (at the plasma edge) $=100$ G, which suggests very good efficiency. A more realistic and detailed analysis, which will include particle simulation[96] and the nonlinear plasma response that is due to the large amplitude excitation is left for a future study.

The second method to accelerate the plasma along the axis is to make use of a rotating electric field produced using two pairs of two facing plates placed around the outer side of the tube in the presence of the divergent field.[11] A rotating field with $m=1$ can be generated by using the two rf power supplies to change the wave phase between the pair of plates. A simple analysis using the rotation of the electric field in the rf frequency range shows that an azimuthal electron current in the plasma can be induced, whereas the ion current is scarcely induced because of the larger inertia of ions. In this calculation, we must consider the penetration depth of the

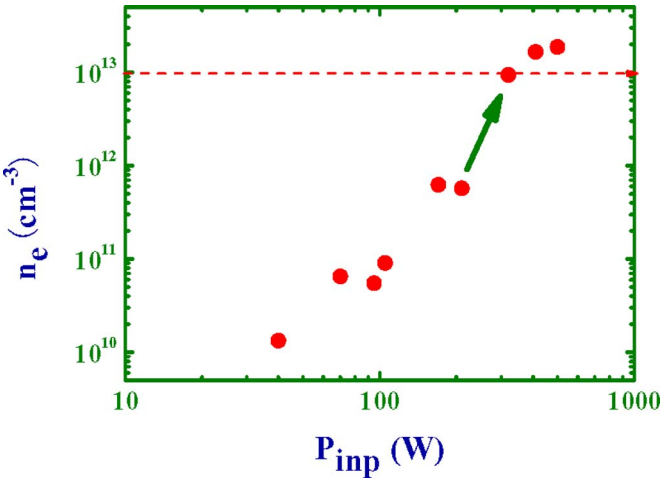

FIG. 10. (Color online) Relationship between n_e and P_{inp} with the use of very small diameter source. Here the applied frequency f is 27. 12 MHz and the magnetic field B is 800 G with an argon gas mass flow rate of 0.5 mg/s. Here, an arrow indicates the transition from ICP to helicon discharge modes.

electric field inside the plasma from the edge. One way to increase the induced electric field is to increase the axial magnetic field.[12]

C. Plasma production and the initial attempt of plasma acceleration

We begin with this section by describing the high-density plasma production. With a short axial length of 4.7 cm due to the insertion of the grounded end plate, an electron density n_e below 10^{12} cm^{-3} with P_{inp}=50 W is achieved, whereas n_e is above 10^{12} cm^{-3} without the end plate.[11] The plasma initiation power is found to be below 20 W with f of $13.56\times m$ MHz (m=2, 3, and 4), by changing the integer m from 1 to 6. This is consistent with the antenna loading calculation[11,12] that indicates that with increasing f, a higher magnetic field is necessary to keep the density constant. Increasing the rf power to 250 W, n_e is close to 10^{13} cm^{-3}, but the density jump is not clear.[12,13] Further increasing power[14,15] up to 500 W by changing the external parameters, we can achieve a density n_e of $\sim 2\times 10^{13}$ cm^{-3}.

Figure 10 shows an example of n_e as a function of P_{inp}. From the data in this figure, two stage transitions can be seen: the first from $\sim 10^{11}$ to $\sim 10^{12}$ cm^{-3}, and the second from $\sim 10^{12}$ to $\sim 10^{13}$ cm^{-3}. These transitions are assigned to the transitions from capacitively coupled plasma (CCP) (Ref. 1) to ICP, and from ICP to helicon plasma, respectively. Note that the particle production efficiency is good, as can be seen from the left bottom data point in Fig. 4, in spite of the short magnetic coil length (in the axial direction) of 10.5 cm.

After the establishment of a high-density helicon plasma, we conducted an initial plasma acceleration trial using the two methods mentioned above. For these experiments, the magnetic field in the helicon plasma generation region is 1.45 kG with the production rf frequency f of 27.12 MHz. With the first method (the multiloop antenna), we increase the exhaust velocity v from below 3000 to close to 4000 m/s by applying an accelerating rf input power up to 160 W with f=6 MHz (production rf power is 400 W with an argon gas flow rate of 0.4 mg/s). However, the weak dependence of v on P_{inp} is found, and there is a tendency that T_e increases while n_e decreases with increasing P_{inp}.

Using the second method (the rotating electric field), we observe in one example an increase in v by several hundred m/s as a result of applying rf input power P_{inp} of 200 W to each plate with f=15 MHz (production rf power is 290 W with an argon gas flow rate of 0.5 mg/s). However, a weak dependence of the wave phase on v is also found, and n_e tends to increase, regardless of the wave phase by this method. Another example, this time shows an increase in v of approximately 2000 m/s with P_{inp} at 220 W and f =10 MHz for each plate (production rf power is 600 W with an argon gas flow rate of 0.5 mg/s). This also shows the weak dependence of v on the wave phase, and a tendency for T_e to increase, while n_e decreases, with increasing P_{inp}.

These initial measurements do not show the electromagnetic propulsion scheme clearly, for reasons that may involve effects of the electrothermal force and the plasma production. The observed phenomena should be characterized in detail, and the optimum method and operating conditions for plasma acceleration need to be found in order to properly demonstrate electrodeless, electromagnetic propulsion.

IV. CONCLUSIONS

We have described unique, high-density helicon plasma sources and have investigated the applications. We have concentrated on describing the characteristics of very large diameter (73.8 cm inner diameter) helicon plasma device LHPD in which plasma of 10^{12}–10^{13} cm^{-3} range can be produced very efficiently. Our experimental results show the scaling properties of the particle production efficiency N_e/P_{inp} up to 10^{15} particles/W. We have found that a simple diffusion model can explain the observed scalings. In particular, our data show that N_e/P_{inp} is approximately proportional to a^2 (L) in the long (short) cylinder cases, which is a valuable guideline in constructing the future helicon plasma sources.

This scaling shows an upper limit for the production efficiency. Since this scaling is based on power balance using a simple diffusion model, it can be applied to general cylindrical, magnetized sources that use other production schemes. Reducing ion collisions in the long cylinder case results in slower radial diffusion, and leads to a production efficiency higher than that obtained from the a^2 scaling. A proposed coefficient is also described herein. Note that the a^2 scaling is valid in the region of $L>k\ a^2$, where k is the coefficient. For $L<k\ a^2$, the L scaling is valid. These results can be derived from Ref. 9.

We investigate plasma performance including the excited wave structures with the low aspect ratio A as low as 0.075 (axial length L is as small as 5.5 cm). The discrete axial mode numbers, which agree with the helicon wave dispersion relation, are found due to the axially imposed boundary conditions. For the B_z component, these conditions are a free, nonconducting boundary at the quartz window, and a fixed, conducting boundary at the termination plate. To investigate the effect of the axial boundary conditions, we plan

to change the termination plates from a punching SUS plate to a flat SUS plate without holes (with and without voltage biasing), and to an insulation plate without holes. Concerning the radial rf wave profile, we find radial modes higher than the fundamental. These findings are expected to contribute to the design of future helicon plasma sources.

For very small diameter (2.5 cm inner diameter) source, from the concept of efficient, longer life electrodeless operation, we successfully produced a high-density helicon plasma with $n_e \sim 10^{13}$ cm^{-3} with a few hundred watts. We also performed an initial trial of two methods of plasma acceleration, both of which utilize the electromagnetic force, which we analyze briefly. More research is necessary both to find the optimum conditions and to demonstrate these new schemes experimentally and theoretically. Conditions necessary to fulfill a concrete space flight plan should be considered afterwards.

The high-density helicon plasma sources developed are expected to play important roles in the evolution of extensive and broad plasma science. Features of high-density (from the low-density) operation, a high ionization degree, and easy and flexible operation over a wide range of external parameters can lead to the use in various fields, including the frontier fields. New concept, new region, and new method applied to the nonlinear plasma research are essential to promote various advanced studies.

ACKNOWLEDGMENTS

Our LHPD experiments were conducted in and supported by the Space Plasma Laboratory, ISAS, JAXA, and we would like to thank Dr. I. Funaki, Dr. S. Sato, Dr. T. Takeda, and Professor K. Yamagiwa for their assistance in carrying out the experiments. This work has been partly supported by the Grants-in-Aid for Scientific Research under Contract Nos. (A) 17206084, (B) 20340163, and (C) 19540524 from the Japan Society for the Promotion of Science.

[1] M. A. Lieberman and A. J. Lichtenberg, *Principles of Plasma Discharges and Materials Processing* (Wiley, New York, 1994).
[2] S. Shinohara, Jpn. J. Appl. Phys., Part 1 **36**, 4695 (1997), and references therein.
[3] R. W. Boswell and F. F. Chen, IEEE Trans. Plasma Sci. **25**, 1229 (1997), and references therein.
[4] F. F. Chen and R. W. Boswell, IEEE Trans. Plasma Sci. **25**, 1245 (1997), and references therein.
[5] S. Shinohara, J. Plasma Fusion Res. **78**, 5 (2002), and references therein (in Japanese).
[6] S. Shinohara and T. Tanikawa, Rev. Sci. Instrum. **75**, 1941 (2004).
[7] S. Shinohara and T. Tanikawa, Phys. Plasmas **12**, 044502 (2005).
[8] T. Tanikawa and S. Shinohara, Thin Solid Films **506–507**, 559 (2006).
[9] T. Tanikawa and S. Shinohara, *E-Proceedings of the 12th International Congress on Plasma Physics*, Nice, 2004 (Association EURATOM-CAE, Cadarache, 2004), Paper No. P2-31, http://hal.archives-ouvertes.fr/hal00002013/en/.
[10] T. Motomura, K. Tanaka, S. Shinohara, T. Tanikawa, and K. P. Shamrai, "Characteristics of large diameter, high-density helicon plasma with short axial length using a flat spiral antenna," J. Plasma Fusion Res. Ser. (in press).
[11] K. Toki, S. Shinohara, T. Tanikawa, I. Funaki, and K. P. Shamrai, *Proceedings of the 28th International Electric Propulsion Conference*, Toulouse (CNES, Paris, 2003), IEPC Paper No. 03-1168.
[12] K. Toki, S. Shinohara, T. Tanikawa, and K. P. Shamrai, *40th AIAA/ASME/SAE/ASEE Joint Propulsion Conference and Exhibit*, Fort Lauderdale, 2004 (American Institute of Aeronautics and Astronautics, Reston, 2004), Paper No. AIAA-2004-39351.
[13] K. Toki, S. Shinohara, T. Tanikawa, and K. P. Shamrai, Thin Solid Films **506–507**, 597 (2006).
[14] K. Toki, S. Shinohara, T. Tanikawa, K. P. Shamrai, T. Hada, I. Funaki, T. Hashimoto, K. Makita, and Y. Ikeda, *Proceedings of the 42nd AIAA/ASME/SAE/ASEE Joint Propulsion Conference and Exhibit*, Sacramento, 2006 (American Institute of Aeronautics and Astronautics, Reston, 2006), Paper No. AIAA-2006-4643.
[15] K. Toki, T. Hashimoto, Y. Tanaka, S. Shinohara, T. Hada, Y. Ikeda, T. Tanikawa, K. P. Shamrai, and I. Funaki, *Proceedings of the 43rd AIAA/ASME/SAE/ASEE Joint Propulsion Conference and Exhibit*, Cincinnati, 2007 (American Institute of Aeronautics and Astronautics, Reston, 2007), Paper No. AIAA-2007-5260.
[16] K. Toki, S. Shinohara, T. Tanikawa, T. Hada, I. Funaki, Y. Tanaka, A. Yamaguchi, and K. P. Shamrai, *Proceedings of the 44th AIAA/ASME/SAE/ASEE Joint Propulsion Conference and Exhibit*, Hartford, 2008 (American Institute of Aeronautics and Astronautics, Reston, 2008), Paper No. AIAA 2008-4279.
[17] K. Toki, S. Shinohara, T. Tanikawa, T. Hada, I. Funaki, K. P. Shamrai, Y. Tanaka, and A. Yamaguchi, "Plasma acceleration in a compact helicon source using RF antennae," J. Plasma Fusion Res. Ser. (in press).
[18] S. Shinohara and H. Mizokoshi, Rev. Sci. Instrum. **77**, 036108 (2006).
[19] J. E. Stevens, M. J. Sowa, and J. L. Cecchi, J. Vac. Sci. Technol. A **13**, 2476 (1995).
[20] S. Shinohara, S. Takechi, and Y. Kawai, Jpn. J. Appl. Phys., Part 1 **35**, 4503 (1996).
[21] S. Shinohara, S. Takechi, N. Kaneda, and Y. Kawai, Plasma Phys. Controlled Fusion **39**, 1479 (1997).
[22] S. Takechi, S. Shinohara, and Y. Kawai, Jpn. J. Appl. Phys., Part 1 **36**, 4558 (1997).
[23] S. Takechi, S. Shinohara, and A. Fukuyama, Jpn. J. Appl. Phys., Part 1 **38**, 3716 (1999).
[24] S. Takechi and S. Shinohara, Jpn. J. Appl. Phys., Part 2 **38**, L1278 (1999).
[25] S. Shinohara and A. Fujii, Phys. Plasmas **8**, 3018 (2001).
[26] K. P. Shamrai and S. Shinohara, Thin Solid Films **506–507**, 555 (2006).
[27] S. Shinohara, N. Matsuoka, and T. Yoshinaka, Jpn. J. Appl. Phys., Part 1 **38**, 4321 (1999).
[28] S. Matsuyama and S. Shinohara, J. Plasma Fusion Res. Ser. **4**, 528 (2001).
[29] S. Shinohara, S. Matsuyama, and N. Matsuoka, Trans. Fusion Technol. **39**, 358 (2001).
[30] S. Matsuyama, S. Shinohara, and O. Kaneko, Trans. Fusion Technol. **39**, 362 (2001).
[31] S. Shinohara, N. Matsuoka, and S. Matsuyama, Phys. Plasmas **8**, 1154 (2001).
[32] S. Shinohara, S. Matsuyama, and O. Kaneko, Thin Solid Films **407**, 209 (2002).
[33] S. Shinohara and S. Horii, Jpn. J. Appl. Phys., Part 1 **46**, 4276 (2007).
[34] S. Shinohara and S. Matsuyama, Phys. Plasmas **9**, 4540 (2002).
[35] S. Shinohara, Y. Nakamura, and S. Horii, Thin Solid Films **506–507**, 564 (2006).
[36] S. Shinohara, Y. Miyauchi, and Y. Kawai, Plasma Phys. Controlled Fusion **37**, 1015 (1995).
[37] S. Shinohara and Y. Kawai, Jpn. J. Appl. Phys., Part 2 **34**, L1571 (1995).
[38] S. Shinohara, Y. Miyauchi, and Y. Kawai, Jpn. J. Appl. Phys., Part 2 **35**, L731 (1996).
[39] S. Shinohara, N. Kaneda, and Y. Kawai, Thin Solid Films **316**, 139 (1998).
[40] S. Shinohara and K. Yonekura, Plasma Phys. Controlled Fusion **42**, 41 (2000).
[41] S. Shinohara and K. P. Shamrai, Plasma Phys. Controlled Fusion **42**, 865 (2000).
[42] K. P. Shamrai and S. Shinohara, Phys. Plasmas **8**, 4659 (2001).
[43] S. Shinohara and K. P. Shamrai, Thin Solid Films **407**, 215 (2002).
[44] M. Ignatenko, M. Azumi, M. Yagi, S. Shinohara, S.-I. Itoh, and K. Itoh, Jpn. J. Appl. Phys., Part 1 **46**, 1680 (2007).
[45] Y. Saitou, A. Yonesu, S. Shinohara, M. V. Ignatenko, N. Kasuya, M. Kawaguchi, K. Terasaka, T. Nishijima, Y. Nagashima, Y. Kawai, M. Yagi, S.-I. Itoh, M. Azumi, and K. Itoh, Phys. Plasmas **14**, 072301 (2007).
[46] K. Terasaka, S. Shinohara, Y. Nagashima, T. Yamada, M. Kawaguchi, T. Maruta, S. Inagaki, Y. Kawai, A. Fujisawa, N. Kasuya, M. Yagi, K. Itoh, and S.-I. Itoh, Plasma Fusion Res. **2**, 031 (2007).
[47] T. Yamada, S.-I. Itoh, T. Maruta, S. Shinohara, N. Kasuya, Y. Nagashima,

M. Yagi, M. Kawaguchi, K. Terasaka, S. Inagaki, Y. Kawai, M. Fukao, A. Fujisawa, and K. Itoh, Plasma Fusion Res. **2**, 051 (2007).
[48]T. Yamada, Y. Nagashima, S. Inagaki, Y. Kawai, M. Yagi, S.-I. Itoh, T. Maruta, S. Shinohara, T. Terasaka, M. Kawaguchi, M. Fukao, A. Fujisawa, and K. Itoh, Rev. Sci. Instrum. **78**, 123501 (2007).
[49]T. Yamada, S.-I. Itoh, K. Terasaka, N. Kasuya, Y. Nagashima, S. Shinohara, T. Maruta, M. Yagi, S. Inagaki, Y. Kawai, A. Fujisawa, and K. Itoh, Plasma Fusion Res. **3**, S1021 (2008).
[50]T. Yamada, S.-I. Itoh, T. Maruta, N. Kasuya, S. Shinohara, Y. Nagashima, M. Yagi, K. Terasaka, S. Inagaki, Y. Kawai, M. Fukao, A. Fujisawa, and K. Itoh, Plasma Fusion Res. **3**, 044 (2008).
[51]T. Yamada, S.-I. Itoh, T. Maruta, N. Kasuya, Y. Nagashima, S. Shinohara, K. Terasaka, M. Yagi, S. Inagaki, Y. Kawai, A. Fujisawa, and K. Itoh, Nat. Phys. **4**, 721 (2008).
[52]Y. Nagashima, S.-I. Itoh, S. Shinohara, M. Fukao, A. Fujisawa, K. Terasaka, Y. Kawai, N. Kasuya, G. R. Tynan, P. H. Diamond, M. Yagi, S. Inagaki, T. Yamada, and K. Itoh, J. Phys. Soc. Jpn. **77**, 114501 (2008).
[53]Y. Nagashima, S-I. Itoh, S. Shinohara, M. Fukao, A. Fujisawa, K. Terasaka, Y. Kawai, N. Kasuya, M. Yagi, S. Inagaki, T. Yamada, and K. Itoh, Plasma Fusion Res. **3**, 056 (2008).
[54]Y. Nagashima, S.-I. Itoh, K. Itoh, A. Fujisawa, S. Inagaki, Y. Kawai, S. Shinohara, M. Fukao, T. Yamada, K. Terasaka, T. Maruta, K. Kamataki, H. Arakawa, M. Yagi, N. Kasuya, G. R. Tynan, P. H. Diamond, Y. Takase, "Reynolds stress measurements for investigation of nonlinear processes of turbulence in the large mirror device and in the large mirror device-upgrade," J. Plasma Fusion Res. Ser. (in press).
[55]T. Yamada, S.-I. Itoh, S. Inagaki, Y. Nagashima, S. Shinohara, T. Maruta, K. Terasaka, K. Kamataki, N. Kasuya, M. Yagi, Y. Kawai, A. Fujisawa, K. Itoh, "Measurement of nonlinear mode couplings in the large mirror device-upgrade," J. Plasma Fusion Res. Ser. (in press).
[56]Y. Nagashima, S.-I. Itoh, S. Shinohara, M. Fukao, A. Fujisawa, K. Terasaka, Y. Kawai, G. R. Tynan, P. H. Diamond, M. Yagi, S. Inagaki, T. Yamada, and K. Itoh, Phys. Plasmas **16**, 020706 (2009).
[57]M. Light, F. F. Chen, and P. L. Colestock, Phys. Plasmas **8**, 4675 (2001).
[58]C. Schröder, O. Grulke, T. Klinger, and V. Naulin, Phys. Plasmas **11**, 4249 (2004).
[59]G. R. Tynan, M. J. Burin, C. Holland, G. Antar, N. Crocker, and P. H. Diamond, Phys. Plasmas **11**, 5195 (2004).
[60]N. Krause, C. Lechte, J. Stöber, U. Stroth, E. Ascasibar, and J. Alonso, Rev. Sci. Instrum. **73**, 3474 (2002).
[61]G. Chen, A. V. Arefiev, R. D. Bengtson, B. N. Breizman, C. A. Lee, and L. L. Raja, Phys. Plasmas **13**, 123507 (2006).
[62]A. M. Keesee and E. E. Scime, Plasma Sources Sci. Technol. **16**, 742 (2007).
[63]M. Krämer, Yu. M. Aliev, A. B. Altukhov, A. D. Gurchenko, E. Z. Gusakov, and K. Niemi, Plasma Phys. Controlled Fusion **49**, A167 (2007).
[64]C. M. Denning, M. Wiebold, and J. E. Scharer, Phys. Plasmas **15**, 072115 (2008).
[65]R. Boivin, S. D. Loch, C. P. Balance, D. Branscomb, and M. S. Pindzola, Plasma Sources Sci. Technol. **16**, 470 (2007).
[66]H. D. Jung, M. J. Park, S. H. Kim, and Y. S. Hwang, Rev. Sci. Instrum. **75**, 1878 (2004).
[67]B. P. Cluggish, F. A. Anderegg, R. L. Freeman, J. Gilleland, T. J. Hilsabeck, R. C. Isler, W. D. Lee, A. A. Litvak, R. L. Miller, T. Ohkawa, S. Putvinski, K. R. Umstadter, and D. L. Winslow, Phys. Plasmas **12**, 057101 (2005).
[68]F. R. Chang-Díaz, Sci. Am. **283**, 90 (2000).
[69]R. M. Winglee, J. Slough, T. Ziemba, and A. Goodson, J. Geophys. Res. **105**, 21067, DOI: 10.1029/1999JA000334 (2000).
[70]T. Ziemba, P. Euripides, J. Slough, R. Winglee, L. Giersch, J. Carscadden, T. Schnackenberg, and S. Isley, Plasma Sources Sci. Technol. **15**, 517 (2006).
[71]C. Charles, Plasma Sources Sci. Technol. **16**, R1 (2007), and references therein.
[72]E. E. Scime, P. A. Keiter, M. M. Balkey, R. F. Boivin, J. L. Kline, and M. Blackburn, Phys. Plasmas **7**, 2157 (2000).
[73]C. S. Corr and R. W. Boswell, Phys. Plasmas **14**, 122503 (2007).
[74]J. Hanna and C. Watts, Phys. Plasmas **8**, 4251 (2001).
[75]N. Hershkowitz, IEEE Trans. Plasma Sci. **26**, 1610 (1998).
[76]T. Tanikawa, S. Shinohara, Y. Ikeda, T. Hada, and K. Toki, Bull. Am. Phys. Soc. **51**, 164 (2006).
[77]T. Tanikawa and S. Shinohara, Proceedings of the International Congress on Plasma Physics, Fukuoka, 2008, p. 281.
[78]T. Tanikawa and S. Shinohara, Bull. Am. Phys. Soc. **53**, 174 (2008).
[79]K. Tanaka, T. Motomura, K. Murakam, and S. Shinohara, Proceedings of the International Congress on Plasma Physics, Fukuoka, 2008, p. 188.
[80]S. Shinohara, K. Tanaka, T. Motomura, and K. Murakami, Bull. Am. Phys. Soc. **53**, 174 (2008).
[81]M. Nisoa, Y. Sakawa, and T. Shoji, Jpn. J. Appl. Phys., Part 2 **38**, L777 (1999).
[82]M. Nisoa, Y. Sakawa, and T. Shoji, Jpn. J. Appl. Phys., Part 2 **39**, L429 (2000).
[83]S. Shinohara and T. Soejima, Plasma Phys. Controlled Fusion **40**, 2081 (1998).
[84]J. Hopwood, Plasma Sources Sci. Technol. **1**, 109 (1992).
[85]F. F. Chen, Plasma Phys. Controlled Fusion **33**, 339 (1991).
[86]K. P. Shamrai, S. Shinohara, V. F. Virko, G. S. Kirichenko, V. M. Slobodyan, and Yu. V. Virko, Plasma Phys. Controlled Fusion **47**, A307 (2005).
[87]S. Shinohara and K. P. Shamrai, Bull. Am. Phys. Soc. **47**, 47 (2002).
[88]H. Takeno, Y. Yasaka, O. Sakai, and R. Itatani, Nucl. Fusion **35**, 75 (1995).
[89]M. Light, I. D. Sudit, F. F. Chen, and D. Arnush, Phys. Plasmas **2**, 4094 (1995).
[90]Y. Sakawa, N. Koshikawa, and T. Shoji, Plasma Sources Sci. Technol. **6**, 96 (1997).
[91]V. F. Virko, K. P. Shamrai, Yu. V. Virko, and G. S. Kirichenko, Phys. Plasmas **11**, 3888 (2004).
[92]K. P. Shamrai and V. B. Taranov, Plasma Sources Sci. Technol. **5**, 474 (1996).
[93]F. F. Chen, M. J. Hsieh, and M. Light, Plasma Sources Sci. Technol. **3**, 49 (1994).
[94]R. W. Boswell, Phys. Lett. **33A**, 457 (1970).
[95]A. Ando, T. Watanabe, H. Tobari, K. Hattori, and M. Inutake, J. Plasma Fusion Res. **81**, 451 (2005) (in Japanese).
[96]Y. Ikeda, T. Hada, S. Matsukiyo, S. Shinohara, and K. Toki, *Proceedings of the 29th International Electric Propulsion Conference*, Princeton, 2005 (Princeton University, Princeton, 2005), Paper No. IEPC-2005-177.